Ab initio studies of possible magnetism in a BN sheet by nonmagnetic impurities and vacancies

Ru-Fen Liu* and Ching Cheng†
Department of Physics, and National Center for Theoretical Sciences, National Cheng Kung University, 70101, Tainan, Taiwan
(Received 11 March 2007; revised manuscript received 19 April 2007; published 6 July 2007)

We performed first-principles calculations to investigate the possible magnetism induced by different concentrations of nonmagnetic impurities and vacancies in a BN sheet. Atoms of Be, B, C, N, O, Al, and Si are used to replace either B or N in the system as impurities. We discuss the changes in the density of states as well as the extent of the spatial distribution of the defect states, the possible formation of magnetic moments, the magnitude of the magnetization energies, and finally the exchange energies due to the presence of these defects. It is shown that the magnetization energy tends to increase as the concentration of the defects decreases in most of the defect systems, which implies a definite preference for finite magnetic moments. The calculated exchange energies are in general tiny but not completely insignificant for two of the studied defect systems, i.e., one with O impurities substituting for N and the other with B vacancies.

DOI: 10.1103/PhysRevB.76.014405 PACS number(s): 75.75.+a, 73.22.−f, 67.57.Pq, 61.72.Ji

I. INTRODUCTION

Magnetism involving only *s*- and *p*-electron elements continues to attract much attention due to the potential for extensive applications as well as the urge to understand its physical origins. Recently, some experimental groups have discovered either weak or strong ferromagnetism in fullerenes[1,2] and graphite systems.[3] A few theoretical studies attempting to find magnetism in some potential nonmagnetic systems have also been carried out previously.[4] However, the origin of ferromagnetism in those systems is still under debate on both the experimental and theoretical sides.[1,5] The mechanism for forming magnetic ordering in solids, such as ferromagnetism, antiferromagnetism, etc., can be referred to direct or indirect exchange interactions (superexchange, double exchange, etc.) among magnetic moments. Therefore, a strong enough exchange interaction should be the crucial criterion determining this possible new class of magnetic materials involving *s*- and *p*-electron atoms. In this work, a boron nitride (BN) sheet is used as the host system and the possible formation of magnetic moments by nonmagnetic defects, including substitution of impurity atoms and creations of vacancies, is studied. The exchange energies of those systems possessing finite magnetic moments are further examined, and we shall demonstrate that there exist mostly very weak interactions among these defect-induced magnetic moments except in two cases.

BN can form three different bulk structures, hexagonal BN (*h*-BN), cubic BN (*c*-BN), and wurtzite BN (*w*-BN). Of these three structures, *h*-BN is the room temperature phase. Similar to graphite, *h*-BN is quasi-two-dimensional (quasi-2D) with weak interaction between layers. Nevertheless, unlike the delocalized π electrons in graphite, the π electrons in BN are distributed more around N, because of its stronger electronegativity. This strong directional effect of bonding confines the motion of the π electrons and thus results in a gap in *h*-BN. BN is the lightest III-V compound of those that are isoelectronic with III-V semiconductors such as GaAs, but with a wider band gap, i.e., $E_g(\mathrm{BN})=4.0-5.8$ eV at room temperature,[6] compared with 1.42 eV of GaAs.

A 2D structural material is usually a good basis for studying the physical properties of the most interesting nanostructures, such as nanotubes, nanoribbons etc.. A tubular structure of BN had been synthesized[7] experimentally. Moreover, it has been shown[8] that, in the different ways of rolling up the BN nanotube, the electronic properties are all semiconducting, as in the extended BN sheet. This is very different from the properties of graphite and carbon nanotubes, which can be either metallic or semiconducting, depending on the method of rolling. Therefore, one would expect that the effects of defects in a BN sheet will indicate many important physical properties that would exist in BN nanotubes.

In semiconducting and insulating systems, magnetic moments can be induced by defects.[9–11] For carbon-related nanomaterials, a recent paper by Andriotis, Sheetz, and Menon[12] analyzed various types of defect in carbon nanotubes and C_{60} polymers and showed the unique rule of carbon vacancies in promoting a magnetic ground state. In this work, two different types of defect are used to study the possible formation of magnetic moments in a BN sheet. One is atoms of Be, B, C, N, O, Al, and Si, used to replace either B or N as impurities. The other is to create vacancies by removing either B or N atoms in the BN sheet. Here, only neutral point defects are considered. Experimentally, it has been shown that the stable defects in bulk hexagonal boron nitride were mostly negatively charged for the defects associated with carbon impurities and nitrogen vacancies.[13] We expect that the magnetic properties induced by charged point defects might be considerably different from the results with neutral ones, as it will be shown later that the filling in the defect bands is important for the formation of finite magnetic moments in these systems.

Our plans for this paper are as follows. Section II summarizes the computational methods in this work. The results of non-spin-polarized calculations are presented in Sec. III. Section III A presents the electronic properties of the BN sheet determined from the analyzed orbital-projected partial density of states (DOS). Section III B includes the effects on the DOS due to defects, i.e., the location of the defect states in the DOS, as well as the extent of the spatial distribution of these defect states. All the results of the spin-polarized calculations are presented in Sec. IV. In Sec. IV A, we investigate the possible formation of finite magnetic moments induced by defects, while the results for exchange energies and

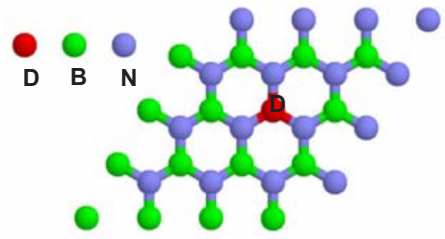

FIG. 1. (Color online) 4×4 unit cell for the hexagonal BN sheet. D represents defects created in the system, i.e., impurities or vacancies.

the corresponding Curie temperatures are presented in Sec. IV B. Finally, the conclusions are in Sec. V.

II. COMPUTATION METHOD

Our calculations are based on density functional theory[14] (DFT) with the generalized gradient approximation (GGA) of Perdew and Wang[15] for the exchange-correlation energy functional. The projector augmented-wave (PAW) method[16] implemented by Kresse and Joubert[17] is used to describe the core-valence electron interactions. There are two, three, four, five, six, three, and four valence electrons included here for Be, B, C, N, O, Al, and Si, respectively. The one-electron Kohn-Sham wave functions are expanded in a plane-wave basis with kinetic energy cutoff (E_{cut} hereafter) of 400 eV. The sampled k points in the Brillouin zone are generated by the Monkhorst-Pack technique[18] with Γ-centered grids for the hexagonal lattice. All calculations are carried out using the Vienna *ab initio* simulation package (VASP).[19]

The calculated lattice constants of h-BN are $a=2.5$ Å and $c=6.36$ Å with $13\times13\times5$ k-point grids, and compare with the experimental results[20] ($a=2.5$ Å and $c=6.66$ Å) reasonably well.[21] Supercells composed of 4×4 primitive unit cells of BN sheet are used to simulate systems with defects (see Fig. 1). The vacuum distance between BN sheets (taken as along the z direction) was chosen to be around 13 Å, which was tested with $3\times3\times1$ k-point grids to be large enough to avoid interactions between the sheets.

For all the relaxed configurations in this work, the atomic forces calculated by the Hellmann-Feynman theorem[23] were smaller than 0.02 eV/Å. In the spin-polarized calculations, we performed the above atomic relaxations again to ensure relaxed configurations. The DOSs and magnetic moments of the final relaxed structures were then evaluated. The magnetic moments presented in this work correspond to the induced magnetic moment per defect, i.e., the integrated spin density $m(r)\equiv n(r)_{\uparrow}-n(r)_{\downarrow}$ of the supercell $M=\int_{supercell}dr\,m(r)$ (μ_B/cell), divided by the number of defects in the supercell. The larger supercells of 8×4 and 8×8 were used to study the possible finite magnetic moments induced by defects, as well as the variation of the magnetization energy (denoted as E_M hereafter) and the exchange energy J with respect to the distances between defects, i.e., defect concentrations.

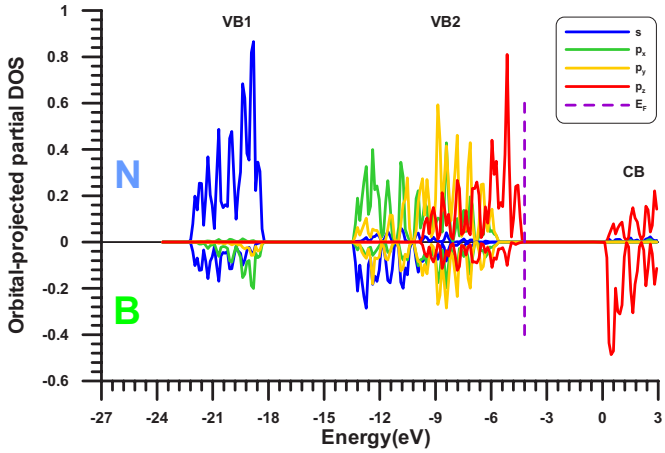

FIG. 2. (Color online) Orbital-projected partial density of states for N and B atoms in hexagonal BN sheet.

III. NON-SPIN-POLARIZED CALCULATIONS: DENSITY OF STATES

A. BN sheet

The orbital-projected partial DOSs of B and N in a BN sheet are presented in Fig. 2. The colors of blue, yellow, green and red in the figures represent the s-, p_x-, p_y-, and p_z-orbital-projected partial DOSs, respectively. The spiky feature of the DOS is due to the dimensional reduction from the 3D bulk h-BN to the 2D planar structure of the BN sheet. Two valence bands (VBs) and the lowest 3 eV range of the conduction band (CB) are included in the figure for discussion. The DOSs in the same energy range for BN sheets with defects will be used in the following discussion for comparison, and the bottom of the CB is taken as the zero of energy for convenience in discussing the splitting of the electronic bands from the two VBs as well as the CB due to the presence of defects. The two VBs in BN sheet are well separated, like those in bulk h-BN.[20] The lower-energy VB (VB1) contains two electrons: one is the s electron of N and the other is from the hybridized s and p electrons (sp^2 electrons hereafter) of B. The higher-energy VB (VB2) contains six electrons, i.e., three sp^2 electrons and one p_z electron from N and two sp^2 electrons from B. From Fig. 2 we see that the two VBs for B are mainly hybridized sp^2 orbitals, while for N VB1 consists of s-like orbitals and VB2 of hybridized sp^2-like orbitals. Near the top of VB2 and the bottom of the CB, the DOSs are mostly p_z-orbital-like. However, the dominant contribution switches from the $p_z$orbital on N atoms near the top of VB2 to the p_z orbital on B atoms near the bottom of the CB. That is, the electronic excitation in the BN sheet involves displacement of electron distribution from the p_z orbital around the N atoms to the p_z orbital around the B atoms.

B. Effect of defects

In the present section, we discuss the effect of defects on the DOS of a BN sheet when the spin polarization is not yet switched on. We shall demonstrate that the effect of defects

on the DOS can be generally categorized into two groups according to the chemical properties of the defects. The 4 $\times$4 supercell was employed in all the results presented in this section, which corresponds to a doping of 1/32 ($\sim$3%) of the defects in the system and a distance of 10.03 Å between neighboring defects. The possible interaction between defects will be discussed in the following section when the exchange energy is investigated. However, the results presented in the present section are applicable to systems with low-density dopings of defects as we shall demonstrate in the following section that the interaction between defects is already quite small in the present configuration. The effect of a C impurity on the DOS of a BN sheet will be discussed in detail first, followed by the results for the series of defects we studied. For simplicity, we denote, e.g., by C_B, the defect system that consists of an impurity of a C atom substituting for one of the B atoms in the original supercell of the BN sheet, and by V_B (V_N) the system consisting of a vacancy replacing one of the original B (N) atoms.

One of the effects of the impurities is to introduce electronic states into the energy regions which originally have no DOS in the BN sheet. We present the total DOSs of all the defect systems considered in this study in Fig. 3. In the case of C_B [Fig. 3(c)], the defect states split from the original three bands and move to the lower-energy region. This is due to the stronger bonding ability of C ions for electrons compared to that of B ions. On the contrary, in the case of C_N, the bonding ability of the C ion is weaker than that of the N ion for electrons, such that the defect bands move to higher-energy positions compared to the original three bands. Therefore, the location of the defect bands is determined by the bonding ability of the defects compared to the substituted host atoms. The effects of defects on the DOSs can be summarized into two types as outlined schematically in Fig. 4. For N_B, C_B, O_B, O_N, and Si_B, the bonding abilities of the impurities are stronger than the substituted host atoms. We name these type I. For Be_B, Be_N, B_N, C_N, Al_N, and Si_N, which are named type II, the three defect bands all move to the region of higher energy than the original three bands.

One can discuss the relative bonding abilities of impurities for electrons by considering the locations of the defect bands in the DOS. When comparing two defect systems with respect to the same substituted host atom, the locations of their defect bands in the gap between VB2 and the CB are used to discuss the order in the bonding abilities of the two impurity atoms. We use Δ to denote the position of the defect band as shown in Fig. 4, i.e., the energy difference between the defect band and the bottom of the CB. The defect system with larger Δ has stronger bonding ability. For the type I systems of C_B and N_B, the order in bonding ability is then C$<$N. Similarly, for the systems of Si_B and C_B, the DOS results lead to the order in bonding ability Si$<$C. In addition, the bonding ability of the O atom is stronger than that of B and N atoms as has already been discussed in the last paragraph. Note that, even though the Δ of the defect band in O_N is zero as it is located at the bottom of the CB, there are still two other defect bands in O_N split from the original VB1 and VB2 to lower-energy regions, and hence O can be considered as exhibiting stronger bonding ability than the N atom. Therefore, the order in bonding ability for the type I

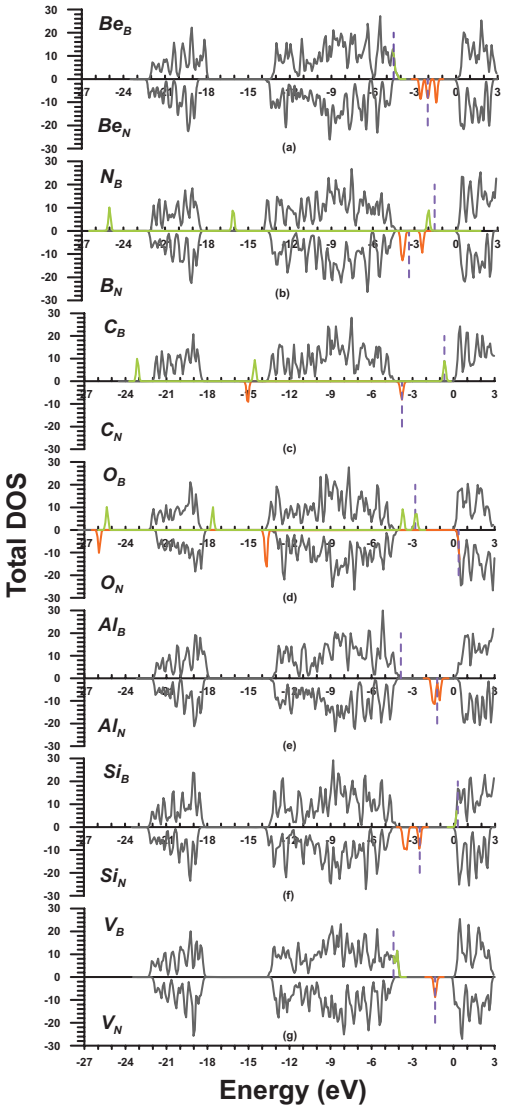

FIG. 3. (Color online) DOSs for the BN sheet with defects. The upper panel in each case shows defects on B while the lower one shows defects on N. (a)–(f) are the results for defect systems with impurities Be, N, B, C, O, Al, and Si atoms, respectively. The defect systems with B and N vacancies are shown in (g). Dashed lines indicate E_F.

systems is Si$<$C$<$N$<$O. A similar discussion can be applied to the type II systems. The order in bonding ability for the type II systems is Al$<$Be$<$B$<$Si$<$C. Note that for the systems of Be_N, B_N, Al_N, and Si_N, which consist of two defect bands in the gap between VB2 and the CB, the one closer to the CB is used as the Δ for sorting the bonding abilities between these defect systems. Combining the above results, one has the order in bonding abilities of these atoms as Al$<$Be$<$B$<$Si$<$C$<$N$<$O. The order in electronegativities for these atoms according to the Mulliken scale is Al (1.37)$<$Be (1.57)$<$B (1.83)$<$Si (2.03)$<$C (2.67) $<$N (3.08)$<$O (3.21),[24] in agreement with the order given by the bonding abilities through considering the locations of defect bands.[25]

Of these studied defect systems, some consist of odd numbers of electrons in the supercell, i.e., Be_B, Be_N, C_B, C_N,

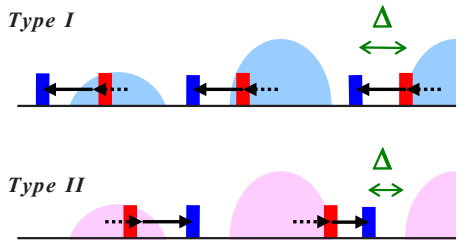

FIG. 4. (Color online) Schematic diagrams of the effect of defects on DOS. The dashed lines show the possible circumstances in forming metal-like DOS.

O_B, O_N, Si_B, Si_N, V_B, and V_N, such that there is an unpaired electron occupying the defect state located between the VB2 and the CB for Be_N, C_B, C_N, O_B, Si_N, and V_N, the top of the VB2 for Be_B and V_B, as well as the bottom of the CB for O_N and Si_B. We denote the state that the unpaired electron occupies as the defect band (DB). We shall show in the next section that magnetic moments are likely to form for those cases with partially occupied DBs. When the partially occupied defect bands which form definite magnetic moments are also extended in nature, long-range magnetic order can develop. Hence, it is expected that for Be_B, O_N, Si_B, and V_B, whose defect states are located at the edge of the original extended bands, the defect bands are more likely to be extended in nature and thus more likely to lead to larger exchange energies, as will be presented in the next section.

In order to determine the properties of the partially filled DBs, the extent of the states in space is established from summing over the contributions of the orbital-projected partial DOSs of the DBs for the neighboring atoms of the defects as presented in Fig. 5. For Be_B, Be_N, O_B, and O_N, we see that the electrons of the DBs are distributed more on the nearest neighboring atoms of the impurity than on the impurity itself. This is contrary to the C_B, C_N, Si_B, and Si_N systems, in which most of the electrons of the DBs are distributed around the impurity atoms. These results demonstrate that the electrons of the defect states due to impurities do not have to be distributed mostly on the impurities themselves. Concerning the spatial extent of the defect states, Fig. 5 shows that only three systems, i.e., Be_B, O_N, and V_N, reach beyond 5 Å. However, the defect states for all the defect systems considered in the present study are confined in a distance of 6 Å around the defects, no matter whether the partially filled defect states are at the edge of the extended bands or not. Finally, we should emphasize that Fig. 5 also reveals two categories of DBs: one is formed by the sp^2-hybridized orbitals, e.g., s, p_x, and p_y, and the other is p_z in nature. These orbital-projected-DOS analyses imply a difference of the electronic distributions of the magnetic moments (detailed discussions in the next section) formed by the unpaired electrons in the DB, e.g., the moments are distributed on the plane of the BN sheet for Be_N, O_B, and V_B, while the moments are distributed perpendicularly to the plane of the BN sheet for the Be_B, C_B, C_N, O_N, Si_B, Si_N, and V_N systems.

IV. SPIN-POLARIZED CALCULATIONS: THE EFFECTS OF DEFECTS

In this section, we present the results of spin-polarized calculations to investigate the possible formation of finite magnetic moments in the BN sheets containing defects as well as the possible long-range magnetic ordering in these systems.

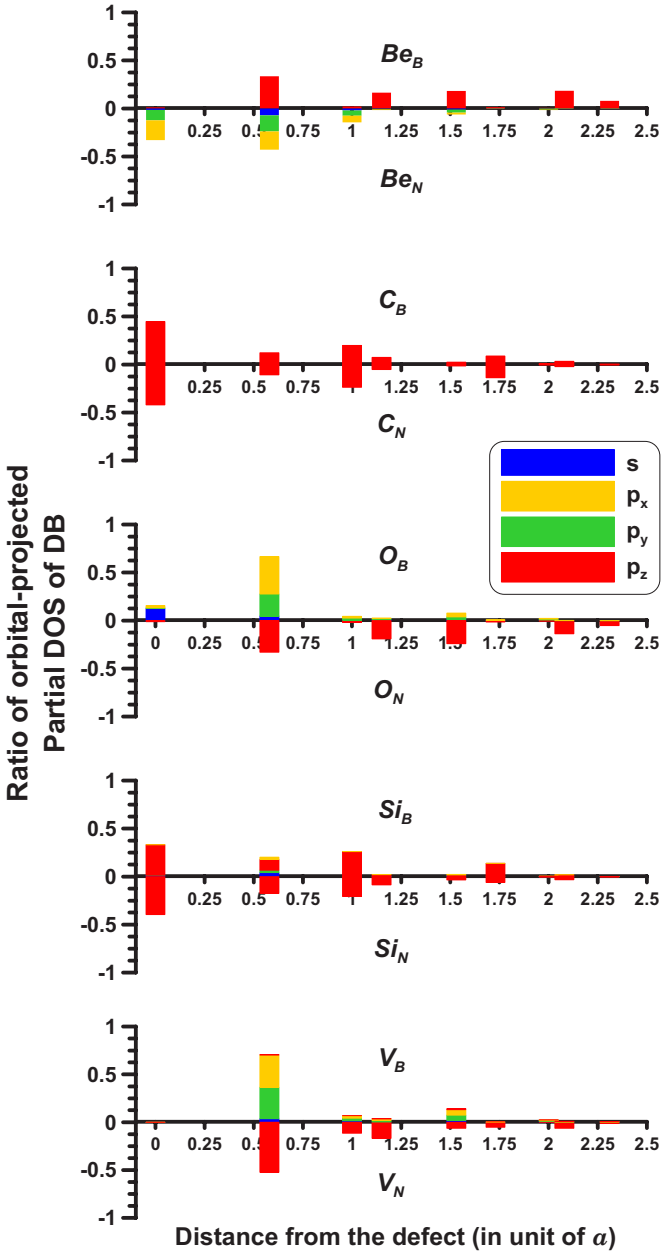

FIG. 5. (Color online) Ratio of the orbital-projected partial DOS summed over the ith nearest neighbors of the defect of a system with partially filled DB. There are one (the defect), three, six, three, six, six, three, three, and one atoms contributing to each bar in sequence. a is the lattice constant 2.5 Å.

A. The possible formation of magnetic moments

To identify the possible magnetic moments due to defects as well as the extent of the magnetic moments, 4×4 and 8×8 supercells consisting of only one defect were employed to simulate the BN sheet with defect concentrations of 3.125% and 0.78%, respectively, i.e., corresponding to a distance of 10.03 and 20.05 Å between nearest-neighbor defects

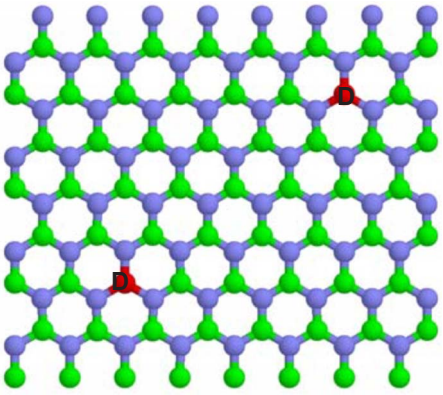

FIG. 6. (Color online) Rectangular supercell with cell dimensions 20.05 and 17.37 Å. The distance between two defect sites is 13.26 Å. The supercell contains 64 primitive cells of the BN sheet.

(denoted by d_D hereafter). In order to obtain the relevant physical quantities for the cases within the range $d_D = 10-20$ Å, we create a rectangular supercell as shown in Fig. 6. By providing either one defect or two defects in the supercell of Fig. 6, one can simulate the cases of 17.37 and 13.26 Å for d_D, respectively. The calculated magnetic moments of the systems with respect to d_D are presented in Fig. 7. For N_B, B_N, Al_B, and Al_N, which have even numbers of electrons in the supercell and completely filled DBs, there exists no magnetization and they are therefore excluded from the following discussions. The calculated magnetic moments in Be_B and V_B were found to vary as d_D increases. However, their magnitudes converge to $1\mu_B$ as d_D increases to 17.37 Å.[26] For Be_N, C_B, C_N, O_B, O_N, Si_B, Si_N, and V_N, the calculated magnetic moments are always found to be $1\mu_B$ and independent of d_D. Note that for all the defect systems possessing finite magnetic moments, the defect bands are always partially occupied. The $1\mu_B$ of magnetization in these defect systems should be attributed to the unpaired electron occupying the defect states.

To understand how stable these finite moments in the BN sheet are, the magnetization energies, i.e., E_M, obtained from the total-energy difference between the systems with and without spin-polarized configuration were calculated. The results are plotted in Fig. 8. First, the E_M's of these systems tend to increase as d_D increase. This suggests a definite preference for finite magnetic moments for those defect systems with distant nonmagnetic defects. Second, the corresponding E_M for those defect systems with distant defects can be determined from the saturated values in the figure, e.g., 360 meV for V_B, 300 meV for O_B, 220 meV for Be_N, etc., and are found to be in a wide energy distribution (from 16 meV for Be_B to 360 meV for V_B). We notice that the defect systems with metal-like electronic properties (Be_B, O_N, Si_B, and V_B), i.e., with Fermi level at the edge of either VB2 or CB, do not necessarily lead to large E_M. For example, the E_M of Be_B is very small, i.e., 16 meV, which is even smaller than the room temperature thermal energy of 25 meV. However, the E_M of V_B is the largest, i.e., 360 meV, of all the systems we considered. We should mention that, when the defect distance is increased, the metal-like DOS

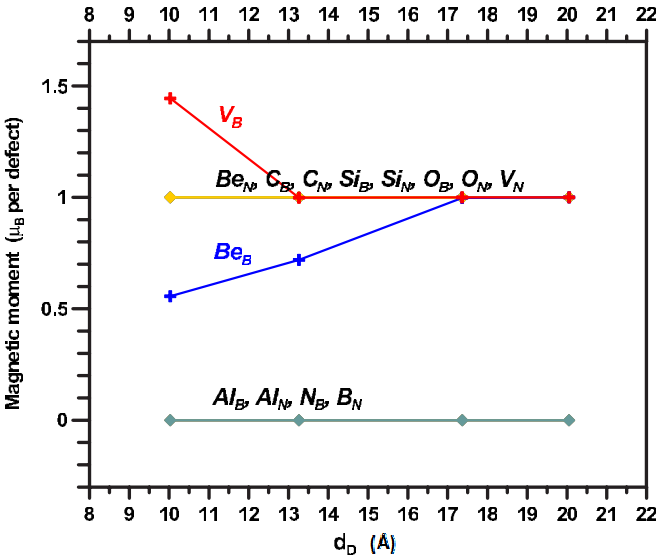

FIG. 7. (Color online) Calculated magnetic moments with respect to d_D, the distance between the nearest-neighboring defects.

does not always hold. The bandwidth of the defect bands might become smaller due to localization, such that they eventually separate from the original VB2 or CB bands. Of the studied systems with metal-like DOS at $d_D = 10.03$ Å, this happens in Si_B and V_B, whose defect bands are originally at the edge of the CB and VB2, respectively. For Be_B and O_N, the defect bands remain at the edge of the VB2 and CB, respectively, up to the largest $d_D = 20.05$ Å we studied.

Finally, for those systems with p_z-like magnetic moments, the bond lengths between defect and neighboring host atoms were found to be relaxed but preserving the threefold symmetry. However, we found that the relaxed bond lengths of Be_N, O_B, and V_B, which have planar distributions in the magnetic moments (an sp^2-hybridized electron in the DB), undergo structural distortions and break the threefold symmetry of the original BN system after the spin-polarization calculation is switched on [Jahn-Teller (JT) effect]. Figure 9 shows the relaxed structure of O_B. The impurity O atom moved toward two of the neighboring N atoms to open up

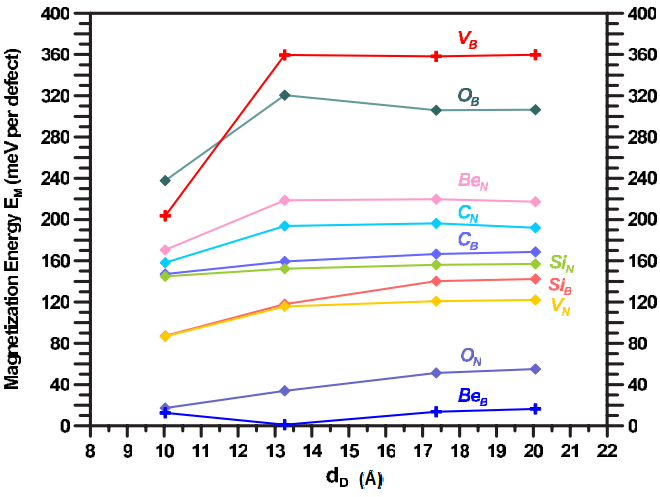

FIG. 8. (Color online) Magnetization energy E_M vs d_D.

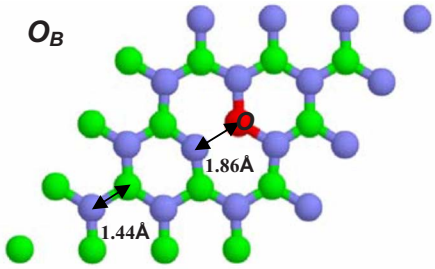

FIG. 9. (Color online) Relaxed structure for the defect system of O_B. The impurity, O atom was relaxed and moved toward two of the three neighboring N atoms to open up one of the original N-O bonds. The spin-polarized energy for this configuration with unequal N-O bond lengths is lower than that with equal N-O bond lengths by 111 meV.

one of the three original N-O bonds. The total energy of this distorted structure with spin polarization is lower than that of the structure with equal N-O bond length by 111 meV; similarly, for Be_N by 33 meV and for V_B by 47 meV. The effect of JT distortion is also responsible for the relatively larger magnetization energy of Be_N, O_B, and V_B with planar-distributed moments compared to systems with p_z-like moments.

B. The exchange energy

By the above analyses, we have demonstrated that nonmagnetic defects can induce finite magnetic moments in a BN sheet. To identify the possible long-range magnetic ordering in these systems, the Heisenberg type of spin coupling[27] is employed to model the interaction (J, i.e., the exchange energy) between the nearest-neighbor magnetic moments due to defects. The exchange energy J is determined from the total-energy difference between two spin configurations, i.e., one with antiparallel and the other with parallel spin configuration, whose energies are denoted as E_{AFM} and E_{FM}, respectively. For simulating two defects at a distance of 10.03 Å, we employed either the 8×4 supercell with two defect sites in each subsupercells of 4×4, or the 8×8 supercell with the sites in the two diagonal subsupercells of 4×4, to generate different spin configurations. In the antiferromagnetic configuration, the 8×4 supercell describes a configuration of six nearest neighbors (d_D=10.03 Å) in which four have spins antiparallel and two parallel to the centered defect, while the 8×8 supercell describes a configuration of two antiparallel-spin nearest neighbors (d_D =10.03 Å) and four next-nearest neighbors with d_D =17.37 Å. The rectangular supercell in Fig. 6 with defects on both sites is also used to simulate the two spin configurations for the systems with defect distance 13.26 Å. In the rectangular supercell, there are four nearest neighbors for a defect and all are antiparallel-spin neighbors in the antiferromagnetic configuration. We have used both 8×4 and 8×8 supercells for the V_B and O_N systems, and the exchange energies obtained from the 8×8 supercells were considered in the discussion as they correspond more to the low-doping conditions we would like to consider. The different values of

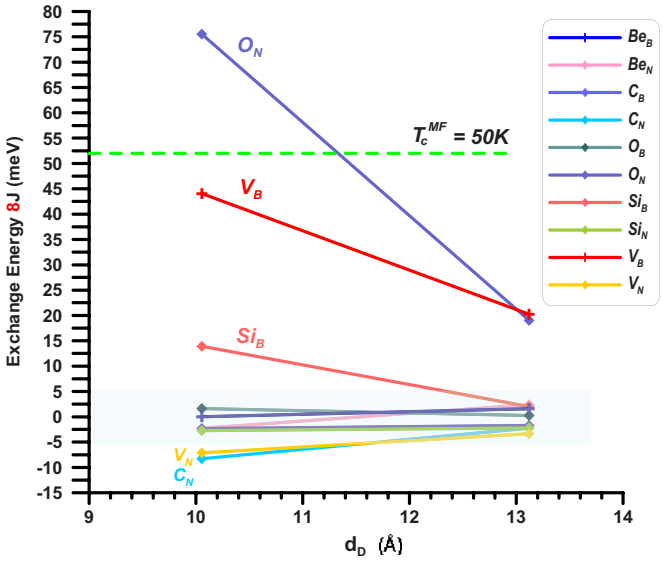

FIG. 10. (Color online) Exchange energy $8J$ vs defect distances where $J\equiv(1/8)(E_{AFM}-E_{FM})$. The energy range from −5 to 5 meV is the estimated region where the magnitude of $8J$ is too small to be used to identify the sign of $8J$ in our calculations. The dashed line indicates the value of exchange energy corresponding to a Curie temperature (T_c^{MF}) of 50 K under the mean-field approximation.

the exchange energies obtained from using 8×4 and 8×8 supercells indicate that the simple pairwise Ising interaction is not a good enough model to describe the energies of these systems of d_D=10.03 Å. We notice that both V_B and O_N have a DB at the edge of either the CB or the VB2. The 8×8 supercells were also used on a few of the other defect systems, but all led to similar results as those obtained from the 8×4 supercells.

Our results are summarized in Fig. 10 where the lines are to guide the eyes. From the previous magnetization energy calculations, our computational accuracy can recognize meaningful energy difference of 5 meV and larger values between configurations. For the systems of Be_B, Be_N, C_B, O_B, and Si_N, the calculated $8J$'s, which are less than 5 meV, are too small to determine whether the systems are ferro- ($8J>0$) or antiferromagnetic ($8J<0$). O_N, V_B, and Si_B are found to be ferromagnetic, and C_N and V_N antiferromagnetic at d_D=10.03 Å. We should mention that the relaxed spin configurations of all the systems discussed here remained antiferromagnetic at the end of the calculations if with initial antiparallel-spin configurations. The exchange energies for O_N, V_B, and Si_B, which possess metal-like DOSs, are relatively larger at d_D=10.03 Å, but not for the case of Be_B whose E_M is tiny anyway. Although the magnetization energy of V_B can be as large as 200 meV at d_D=10.03 Å, the exchange energy is considerably smaller (5.6 meV); similarly for Si_B, whose $E_M\sim90$ meV while J is smaller than 2 meV. (Note that Fig. 10 shows the data for eight times the exchange energy J.) This contrast is much reduced in the case of O_N, whose $E_M\sim17$ meV and $J\sim9.4$ meV at d_D =10.03 Å. When d_D is increased to 13.26 Å, the magnitude of the exchange energies for all the above systems decreases. Finally, there are only two systems, i.e., O_N and V_B, which have large enough exchange energies to be identified numerically as magnetically ordered systems.

Within the framework of the Heisenberg spin model, it is possible to estimate the Curie temperatures (T_c) of these systems. The mean-field result is given by

$$k_B T_c^{MF} = \frac{2}{3}\bar{J}_0, \tag{1}$$

where $\bar{J}_0$ is the on-site exchange parameter reflecting the exchange field created by all the neighboring magnetic moments.[28,29] Note that the T_c determined by Eq. (1) is regarded as an overestimated value.[30] Since the physics of T_c involves the disordered nature of the system due to temperature, $\bar{J}_0$ should be related to the energy difference between the local disorder state and the ferromagnetic state of the system.[29] However, the exchange energies obtained here do not include the disorder effect, i.e., E_{AFM} is calculated from the ordered antiferromagnetic configuration. Hence, the estimated T_c (denoted as $\tilde{T}_c^{MF}$) obtained by just simply substituting J in Fig. 10 for $\bar{J}_0$ in Eq. (1) is expected to be an upper bound of T_c^{MF} for a given system. For O_N, V_B, and Si_B with relatively large J's at d_D=10.03 Å, the $\tilde{T}_c^{MF}$'s are 72, 43, and 13 K, respectively. However, they are reduced to around 20 K for O_N and V_B and below 5 K for Si_B when d_D is increased to 13.26 Å. In addition, the $\tilde{T}_c^{MF}$'s of the defect systems with exchange energies smaller than 5 meV are all below 5 K in different concentrations. Therefore, one can conclude that the effect of the long-range magnetic ordering is very weak in all the defect systems considered here except for the defect systems of O_N and V_B. However, our calculations suggest that the systems of Be_N, C_B, C_N, O_B, O_N, Si_B, Si_N, V_B, and V_N all have finite magnetic moments and are therefore at least paramagnetic.

V. CONCLUSIONS

Different concentrations of nonmagnetic impurities and vacancies in a BN sheet were studied using first-principles methods to investigate the possible magnetism in these systems involving only *s*- and *p*-electron elements. We first studied the effects of these defects on the DOS and analyzed the character as well as the spatial extent of these defect states. The magnetization energies and possible magnetic moments as well as the exchange energies for these defect systems in different concentrations were evaluated. We demonstrated that all the defect systems with partially filled defect bands exhibited a definite preference for finite magnetic moments. The calculated exchange energies for low-density defect systems are all tiny except for O_N and V_B, whose exchange energies are not completely insignificant with an estimated T_c of 20 K.

ACKNOWLEDGMENTS

This work was supported by the National Science Council of Taiwan. Part of the computer resources were provided by the NCHC (National Center of High-Performance Computing). We also acknowledge the support of NCTS (National Center of Theoretical Sciences) through the CMR (Computational Material Research) focus group.

*Electronic address: fmliu@phys.ncku.edu.tw
†Electronic address: ccheng@phys.ncku.edu.tw

[1] T. L. Makarova *et al.*, Nature (London) **413**, 716 (2001). However, there is a retraction in T. L. Makarova *et al.*, *ibid.* **440**, 707 (2006), and references within.
[2] M. Tamura *et al.*, Chem. Phys. Lett. **186**, 401 (1991); P. M. Allemand *et al.*, Science **253**, 301 (1991); Y. Murakami and H. Suematsu, Pure Appl. Chem. **68**, 1463 (1996); F. J. Owens, Z. Iqbal, L. Belova, and K. V. Rao, Phys. Rev. B **69**, 033403 (2004); O. E. Kvyatkovskii, I. B. Zakharova, A. L. Shelankov, and T. L. Makarova, *ibid.* **72**, 214426 (2005).
[3] P. Esquinazi, A. Setzer, R. Höhne, C. Semmelhack, Y. Kopelevich, D. Spemann, T. Butz, B. Kohlstrunk, and M. Lösche, Phys. Rev. B **66**, 024429 (2002); P. Esquinazi, D. Spemann, R. Hohne, A. Setzer, K. H. Han, and T. Butz, Phys. Rev. Lett. **91**, 227201 (2003); Y. Kopelevich *et al.*, J. Low Temp. Phys. **119**, 691 (2000).
[4] Yong-Hyun Kim, J. Choi, K. J. Chang, and D. Tomanek, Phys. Rev. B **68**, 125420 (2003); Yuchen Ma *et al.*, New J. Phys. **6**, 68 (2004); H. J. Xiang *et al.*, *ibid.* **7**, 39 (2005); Hong Seok Kang, J. Phys. Chem. B **110**, 4621 (2006); R. Q. Wu *et al.*, J. Phys.: Condens. Matter **18**, 569 (2006); M. S. Si and D. S. Xue, Europhys. Lett. **76**, 664 (2006).
[5] A. N. Andriotis, M. Menon, R. M. Sheetz, and L. Chernozatonskii, Phys. Rev. Lett. **90**, 026801 (2003); P. Esquinazi, D. Spemann, R. Hohne, A. Setzer, K. H. Han, and T. Butz, *ibid.* **91**, 227201 (2003); P. O. Lehtinen, A. S. Foster, Y. Ma, A. V. Krasheninnikov, and R. M. Nieminen, *ibid.* **93**, 187202 (2004).
[6] S. L. Rumyantsev *et al.*, in *Properties of Advanced Semiconductor Materials GaN, AlN, InN, BN, SiC, SiGe*, edited by M. E. Levinshtein, S. L. Rumyantsev, and M. S. Shur (John Wiley and Sons, New York, 2001), pp. 67–92.
[7] J. Cumings and A. Zettl, Chem. Phys. Lett. **316**, 211 (2000); E. Bengu and L. D. Marks, Phys. Rev. Lett. **86**, 2385 (2001); W. Mickelson, S. Aloni, W. Han, J. Cumings, and A. Zettl, Science **300**, 467 (2003); F. F. Xu, Y. Bando, and D. Golberg, New J. Phys. **5**, 118 (2003).
[8] X. Blase, A. Rubio, S. G. Louie, and M. L. Cohen, Europhys. Lett. **28**, 335 (1994).
[9] J. Osorio-Guillén, S. Lany, S. V. Barabash, and A. Zunger, Phys. Rev. Lett. **96**, 107203 (2006).
[10] D. M. Edwards and M. I. Katsnelson, J. Phys.: Condens. Matter **18**, 7209 (2006).
[11] A. N. Andriotis, R. M. Sheetz, and M. Menon, J. Phys.: Condens. Matter **17**, L35 (2005).
[12] A. N. Andriotis, R. M. Sheetz, and M. Menon, Phys. Rev. B **74**, 153403 (2006).
[13] A. Katzir, J. T. Suss, A. Zunger, and A. Halperin, Phys. Rev. B **11**, 2370 (1975), and references therein.
[14] P. Hohenberg and W. Kohn, Phys. Rev. **136**, B864 (1964); W.

Kohn and L. J. Sham, Phys. Rev. **140**, A1133 (1965).

[15] J. P. Perdew, in *Electronic Structure of Solids '91*, edited by P. Ziesche and H. Eschrig (Akademie-Verlag, Berlin, 1991); J. P. Perdew, J. A. Chevary, S. H. Vosko, K. A. Jackson, M. R. Pederson, D. J. Singh, and C. Fiolhais, Phys. Rev. B **46**, 6671 (1992).

[16] P. E. Blöchl, Phys. Rev. B **50**, 17953 (1994).

[17] G. Kresse and D. Joubert, Phys. Rev. B **59**, 1758 (1999).

[18] H. J. Monkhorst and J. D. Pack, Phys. Rev. B **13**, 5188 (1976).

[19] G. Kresse and J. Hafner, Phys. Rev. B **47**, 558 (1993); **49**, 14251 (1994); G. Kresse and J. Furthmuller, Comput. Mater. Sci. **6**, 15 (1996); Phys. Rev. B **54**, 11169 (1996).

[20] N. Ooi, A. Rairkar, L. Lindsley, and J. B. Adams, J. Phys.: Condens. Matter **18**, 97 (2006).

[21] The lattice constants calculated from the local density approximation (LDA) with E_{cut}=400 eV are a=2.48 Å and c=5.9 Å and become a=2.5 Å and c=6.23 Å when E_{cut} is increased to 500 eV. However, the GGA result for c becomes 7 Å at E_{cut} =500 eV. Similar results of overestimation for c in hexagonal BN from the GGA have been doccumented in Refs. 20 and 22.

[22] A. Janotti, S.-H. Wei, and D. J. Singh, Phys. Rev. B **64**, 174107 (2001).

[23] H. Hellmann, *Einführung in die Quantenchemie* (Deuticke, Leipzig, 1937), pp. 61, 285; R. P. Feynman, Phys. Rev. **56**, 340 (1939).

[24] J. E. Huheey, E. A. Keiter, and R. L. Keiter, *Inorganic Chemistry: Principles of Structure and Reactivity*, 4th ed. (HarperCollins, New York, 1993).

[25] In addition to the Mulliken scale, the Pauling scale is another commonly used definition for the electronegativity of an atom. According to the Pauling scale, the order is Be (1.57) < Al (1.61) < Si (1.9) < B (2.04) < C (2.55) < N (3.04) < O (3.44) (Ref. 24) in which the order of Be < Al and Si < B is opposite to that of the Mulliken scale. However, the electronegativity difference between Al and Be atoms is comparatively smaller than that of any other two elements of the list, and the order is expected to be switched due to other possible effects in the system, e.g., the type of atoms they bind, and similarly for Si and B atoms.

[26] The spin-polarized calculations by using the LDA gave zero magnetic moment for Be_B, $1.6\mu_B$ per defect for V_B, and $1\mu_B$ per defect for Be_N, C_B, C_N, O_B, O_N, Si_B, Si_N, and V_N at d_D =10.03 Å. When d_D is increased to 20.05 Å, the magnetic moment of Be_B increases to $0.98\mu_B$ per defect, while that of V_B decreases to $1\mu_B$ per defect. The direction of changes resembles that in GGA calculations as shown in Fig. 7. Hence, the behavior of forming finite magnetic moments of these defect systems calculated from the LDA is consistent with that from the GGA.

[27] With the Heisenberg Hamiltonian: $H=-2J\Sigma_{ij}\mathbf{S}_i\cdot\mathbf{S}_j$, we have $\xi J \equiv E_{AFM}-E_{FM}$, where ξ is the effective number of coupling pair per defect.

[28] K. Sato, P. H. Dederics, and H. Katayama-Yoshida, Europhys. Lett. **61**, 403 (2003).

[29] J. Kudrnovský, I. Turek, V. Drchal, F. Máca, P. Weinberger, and P. Bruno, Phys. Rev. B **69**, 115208 (2004).

[30] G. Bouzerar, T. Zinman, and J. Kudrnovský, Europhys. Lett. **69**, 812 (2005).